Hydrodynamic performances of gully with air-water flows in drainage system

S.W. Chang* **Department of Marine Engineering, National Kaohsiung Marine University, Taiwan**

D.C. Lo **Department of Maritime Information and Technology, National Kaohsiung Marine University, Taiwan**

H.F. Liu **CU Golden Power Products, Inc, Taiwan**

J.S. Liou **Department of Maritime Information and Technology, National Kaohsiung Marine University, Taiwan**

* Corresponding author email: swchang@mail.nkmu.edu.tw; Tel: +886-7-8100888ext.5216

(Received 21th February 2014, accepted 31th March 2014)

Abstract

This study examines the hydrodynamic performances of a gully designed for building drainage system. The transient variations of free surface, fluid velocity and static pressure in the gully with twin air-water inlets are numerically analyzed by adopting turbulence model(s) to attack the moving boundary problem. Experimental test results reconfirm the numerical predications with the maximum capacities and the oscillating airflow pressures detected. Flow images illustrating the interfacial air-water flow structures at various test conditions are presented. Particularly, as an attempt to improve the measurement quality for the self-depuration capacity specified in EN 1253-2:2002, which has been widely adopted as the international standard for testing the hydrodynamic performance of gullies with building applications, the optical measurement method is newly devised and described in details. The favorable numerical and experimental results confirm the applicability of present gully in a modern drainage system for preventing odour transmissions.

Keywords: Hydrodynamics Air-water Two-phase Flow, Drainage, Building.

Nomenclature

English symbols

A fractional flow areas (m^2)
b flow losses in porous media or across porous baffle plates ($m\ s^{-2}$)
d entry tube diameter (m)
f viscous accelerations term ($m\ s^{-2}$)
G acceleration rates of fluid particles ($m\ s^{-2}$)
L lumen
P static pressure (Pa)
Q volume flow rate ($L\ min^{-1}$)
Re_L Reynolds number of liquid flow for mixed entry water = $\rho_L V_L d/\mu_L$
V_F fractional flow volume ($m^3\ s^{-1}$)
V_L mean liquid flow velocity for mixed entry water ($m\ s^{-1}$)
u,v,w fluid velocities in x,y,z direction ($m\ s^{-1}$)
x,y,z coordinates (m)

Greek symbols

α void fraction of entry flow
ρ_L density of liquid flow for mixed entry water ($kg\ m^{-3}$)
μ dynamic viscosity of liquid flow for mixed entry water ($kg\ s^{-1}\ m^{-1}$)

Subscripts

A flow entry A
B flow entry B

1.Introduction

Efficient transportation of mixed water from a variety of appliances connecting with the vertical stack in a building for a modern drainage system requires multi-discipline research efforts. As the mixed water flow in a drainage system involves complex air-water interfacial mechanisms, the sufficient discharging capacities with the capability of preventing the foul odors ingress into the habitable spaces within the allowable acoustic limits propose considerable challenge for the architecture designers. With random and intermittent falling water streams into the vertical stack via the discharge branches, the entrained airflow by the water stream yields the water discharge into the complex air-water two-phase flow taking a variety of interfacial patterns. The types of local interfacial flow structures for such mixed water are affected by the geometry of the pipe line/appliance, the flow rate of mixed water, the location where the appliance is installed and the type of discharge. In compliance with the design code of a drainage system, the common two-phase flow patterns in a branch and the stack are the stratified/wavy and the annular flows respectively. As the branch discharge is often a random and intermittent process, the stratified/wavy flows through a drainage system inherit the intermittent

characteristic as the transient phenomena [1]. Over the air-water interfaces, the air movements are induced by the interfacial shear forces on the free surfaces of the moving mixed water; which locally trigger the positive or negative transient air pressures and propagate through the stack and branches of the entire drainage system [2]. Moreover, the transient propagation of air pressures at sonic speed is affected by the local air-water interfacial structure and the reflection and transmission at the flow boundaries. Very complicate two-phase flow phenomena signify the hydrodynamic performances of a drainage system, which also determine the transient propagation of airflow pressures through the drainage network. Particularly, the blockage of a high momentum air stream by the water curtain or the water excursions in a drainage system often diminishes a trap seal due to the water hammer effect [3]. Nevertheless, the propagation of positive or negative transient pressures, which interdependently affect the interfacial structures and the airflow velocities, could cause unfavorable acoustic effect, limit the maximum discharge capacity and damage the trap seals in a drainage system.

To prevent foul odors ingress into the habitable spaces through the interconnected drainage network in a building, it is a common practice to install the water seals at locations where appears as appropriate. However, triggered by the various and complex air-water interfacial actions along the interconnecting pipe works of a drainage system, the stimulated airflow pressure waves, which generally transmit at sonic speed, can damage these water seals. In this regard, the requirement for a trap seal with about 50mm water height is typical so that the permissible pressure excursions for a drainage system is generally determined as ±375 Nm^{-2} [1-2]. As an attempt to suppress the pressure surges in a drainage system, Swaffield et al [4] simulated the propagation of air pressure transients in the drainage system by solving the St. Venant equations using finite difference scheme; while the positive or negative pressure reflections at the interfacial boundaries were embodied in the airflow momentum equation via the friction coefficient to account the manifesting shearing drag in the airflow. Due to the complicate two-phase air-water flow phenomena in each appliance, branch, junction and the stack of a drainage system, the suppression of undesirable pressure transients through a drainage system remains as a formidable task. Particularly the influences of the various two-phase flow phenomena in each component and appliance of a drainage system on the hydrodynamic performances of a drainage system are interdependent. As a result,

various research works are motivated with their particular aims at optimizing the performances of the sub-assemblies in a drainage system with attendant innovative drainage components devised. In this respect, the vortex fin [3] was installed at the elbow bend of a vertical stack to stabilize the airflow pressures by suppressing the positive pressure surges caused by the water curtain downstream the middle section of the elbow-bend. As the water seal in a gully can prevent the transmission of odors ingress through the interconnected networks of a drainage system at any selected junction, several types of gully were patented [5-12] and tested for providing the stable water seal at a multiple junction in a drainage system. In [6], the hydrodynamic characteristics of a gully were reported using a set of numerical results. Within the framework of the lumped bubbly flow model, the geometries of entry/discharge ports and the plenum chamber of a gully were shown as the predominant factors determining the air-bubble dynamics and thus the oscillating pressures in a gully [6].

Relevant researches for the hydrodynamic performances and the associated air-water interfacial mechanisms in a gully are very rare [5, 15], leading to the insufficient revelation for the influences of gully geometry, entry void fraction of mixed water and the air-water flow rate on its hydrodynamic performances. However, due to the widespread usages of gully in modern drainage systems for buildings, European Council has regulated EN 1253-2 standard [13] in 2002 for testing the hydrodynamic performances of a gully. In Gullies for buildings – Part 2: Test methods, the testing guidelines for load, water seal, blockage prevention, thermal behavior, tightness and flow rate are regulated [13]. Among the various test methods specified by EN 1253-2, the self-cleaning performance of a gully is tested by drifting solid spheres in the air-water flow through the gully. As water is the commonest solvent for many odor ingredients, the influence of localized small-scale recirculation zones in a gully, which impede the replenishment of fresh mixed water through a gully, on the self-depuration performance cannot be quantitatively identified. As an attempt to quantitatively assess the self-depuration performance of a gully, a newly devised optical testing method is presented with its testing characteristics examined. Using the patented triple-entry gully as an illustrating specimen, the test results determined from the newly devised optical assessment for self-depuration performance as well as the associated hydrodynamic performances of the gully are numerically and experimentally

examined.

2. Experimental and numerical details

2.1 Experimental facilities

Figure 1 depicts (a) test facilities with detailed illustrations for the optical device measuring the self-depuration performance (b) transparent test gully. As shown by Fig. 1(a), water fed from tank (1) which locates at fifth floor of a building to provide 13 m of water height is guided through a vertical stack (2) to the test gully (3). Complying with the design code for the single-pipe vertical stack in a building drainage system, an air admitting valve (4) is installed on top of the vertical stack. When water stream flows inside the vertical stack to entrain airflow in the drainage pipeline, the airflow pressure is controlled in the typical range of ±375 Nm^{-2} via the auto air entrainment through the air admitting valve (4). Similar to the practical conditions, the mixed water (air-water) flows are established prior to entering the test gully (3). Net volume of the water flow through the test gully (3) during a test period is measured by the downstream water tank (5) with the time span detected by the electronic timer. The method adopted to detect the water flow rate complies with the method of water flow rate measurement regulated by CNS14431 Q3001 [14]; which enables the measurement of the averaged volume flow rate of water through the test gully (3). A scale is attached along the inner periphery of each transparent inlet pipe (6)(7) connecting with the test gully (3). As the stable stratified air-water flow in the basically horizontal inlet pipe (6)(7) is emulated by this test facility, the void fraction (α) of entry mixed water can be determined in according to the water level measured from each inlet pipe (6)(7). The air-water flow structures in the gully (3) at each tested Re_L with single and/or twin entry flows are visualized from the snapshots collected by the CCD image system (8). This imaging system can record the flow image at 300 fps with 600 pixels per gully width. The CCD camera (8) is aimed at the angle normal to the test gully (3) at a constant focal length. Locations of the light sources are individually adjusted for each test condition. As indicated in Fig. 1, the static airflow pressure is detected by a computerized digital micro manometer with the precision of 0.01 mm-H_2O (9). The pressure measurements are simultaneously performed with the flow visualization tests with the temporal variation of flow pressures detected/stored by the on-line data acquisition system. Depending on the sensing location and the hydrodynamic performance of the test gully (3), the agitating air bubbles and/or

pressure waves triggered by the unstable interfacial surface could stimulate pressure fluctuations. The detailed temporal variation of the airflow pressure at each test condition is recorded and stored by present measurement unit for analyzing the hydrodynamic performance of the test gully and validating the numerical results.

The constructional details of the of present test gully show several distinct features designed for improving the hydrodynamic performances, Fig. 1(b). This gully is configured by a cylindrical plenum chamber (1) within which a nozzle shaped core (2) directs the accelerated mixed water stream from the twin perpendicular inlet ports (3)(4) toward the inclined base (5). As depicted by Fig. 1(b), the inclination of base plate (5) is designed to guide the mixed water stream toward the exit port (6). Cross-section area of the exit port (6) is equal to the sectional annular area between the nozzle core (2) and the cylindrical outer casing (7). A filter leaf (8) is installed on the top of the gully assembly. Although such open contact with atmosphere adds another pathway for airflow entrainment, it remains as a common practice in many countries for discharging bathroom/kitchen waste water by fitting a filter leaf on the floor to connect with the drainage system. An optional segregation plate (9) in the nozzle core (2) can also be installed to separated the mixed water streams from the two perpendicular inlet ports (3)(4). It is noticed that a streamlined bump (10) is installed at the base of the exit port (6). This design concept follows the typical practice for stabilizing the open channel flow upstream the bump installed on the river bank. The favorable impacts of the streamlined bump (10) for stabilizing the mixed water flow through present test gully will be later demonstrated using the experimental /numerical results.

To quantitatively assess the self-depuration performance for each test gully, the normalized lumen level through the test gully at each test condition is detected by present computerized optical system. As shown by Fig. 1(a), the light source emits light through the test gully, within which the mixed water flows, toward the optical receiver (10). The optical receiver (10) is positioned at the opposite side of the light source to transmit the received light signal to the PC via the converter (11). By way of feeding the mixed water at the particular test condition defined by Re_L and α, the reference lumen levels at the pure water flow condition (L_1) are initially detected. It is worth noting that the air bubbles emerging in the water trap of each test gully reflect light and affect the light deflection. Thus the instant lumen values

at the pure-water test conditions oscillate about L_1 reference and depend on the interfacial properties of the water trap in the test gully, which are geometry, Re_L and α dependent. However, the temporal lumen variations at the pre-defined pure mixed water (clean) entry conditions are detectable by present optical unit so that the L1 references for the particular test gully are pre-determined. Prior to feeding the mixed water into the test gully for self-depuration performance test, the water trap stored in the test gully is dyed by the black ink with the lumen level (L_0) detected. With the same light source and optical receiving unit, the L0 level at each "dark" test condition is controllable by adjusting the equivalent concentration of ink and appears as a stable reference due to the absence of air bubble prior to feeding the mixed water into the test gully. After charging the mixed water into the test gully, the lumen level starts rising from L_0 toward L_1. The detailed temporal lumen variation from L_0 to L_1 represents the self-depuration performance of the test gully and is recorded by present optical unit. The time required for the detected lumen level from L_0 to 99% of L_1 is defined as the self-depuration time (T). As an illustrative example, Fig. 1(c) depicts a typical temporal lumen variation from L_0 to L_1 with the single mixed water entry flow at the test condition of ReL (α) = 10589 (0.56). As indicated by Fig. 1(c), the instant lumen value for this particular test gully increases from L_0 toward L_1 as time goes by. The temporal lumen values oscillate about L_1 reference after the time lapse exceeds T due to the presence of air bubbles in the water trap of test gully. With each tested gully of different geometries or different flow rates, the L_0 and L_1 references are accordingly varied. The temporal normalized lumen variation in terms of L/L_1 is adopted to quantitatively characterize the self- self-depuration performance of a gully. To clarify the air-water entry conditions, the void fractions for present mixed-water flows are detected with the results presented in Figs. 1(d) and 1(e). As the water flow rate increases, the void fraction keeps reducing, Figs. 1(d) and 1(e). Due to the differential entry angles for A, B entry pipes, the void fractions detected from entry A are consistently higher than the B-entry counterparts for both single- and twin-entry flows.

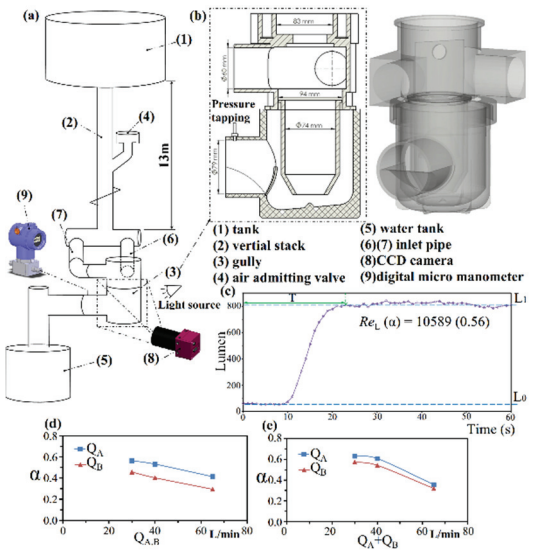

Fig. 1 (a) experimental test facilities (b) test gully (c) typical temporal lumen variation from L_0 to L_1 with single mixed water entry flow at test condition of Re_L (α) = 10589 (0.56); variations of void fraction against entry flow rate with (d) single (e) twin flow entry.

2.2 Numerical method

Present simulations for determining the fluid velocities and pressures are based on Navier-Stokes equations using FLOW-3D commercial code. By assuming water as incompressible fluid with unchanged viscosity, the governing flow equations for Newtonian fluid are expressed as follows:

Continuity equation:

$$\frac{\partial u}{\partial x}+\frac{\partial v}{\partial y}+\frac{\partial w}{\partial z}=0 \qquad (1)$$

Momentum equations

$$\begin{aligned}
&\frac{\partial u}{\partial t}+\frac{1}{V_F}\left\{uA_x\frac{\partial u}{\partial x}+vA_y\frac{\partial u}{\partial y}+wA_z\frac{\partial u}{\partial z}\right\}\\
&\quad=-\frac{1}{\rho}\frac{\partial P}{\partial x}+G_x+f_x-b_x-\frac{R_{SOR}}{\rho V_F}(u-u_w-\delta u_s)\\
&\frac{\partial v}{\partial t}+\frac{1}{V_F}\left\{uA_x\frac{\partial v}{\partial x}+vA_y\frac{\partial v}{\partial y}+wA_z\frac{\partial v}{\partial z}\right\}\\
&\quad=-\frac{1}{\rho}\frac{\partial P}{\partial y}+G_y+f_y-b_y-\frac{R_{SOR}}{\rho V_F}(v-v_w-\delta v_s)\\
&\frac{\partial w}{\partial t}+\frac{1}{V_F}\left\{uA_x\frac{\partial w}{\partial x}+vA_y\frac{\partial w}{\partial y}+wA_z\frac{\partial w}{\partial z}\right\}\\
&\quad=-\frac{1}{\rho}\frac{\partial P}{\partial z}+G_z+f_z-b_z-\frac{R_{SOR}}{\rho V_F}(w-w_w-\delta w_s)
\end{aligned} \qquad (2)$$

where V_F is the fractional flow volume treated as a mass source. A_x, A_y and A_z are the fractional flow areas in x, y and z directions, respectively. In equations (1) and (2), u, v, w refer to the velocity components in x, y, z coordinate directions; P refers to static pressure, while ρ and ν refer to the density and kinematic viscosity coefficients of the fluids respectively. G_x, G_y, G_z refer to the acceleration rates of fluid particles. f_x, f_y, f_z are the viscous accelerations terms; whereas b_x, b_y, b_z refer to the flow losses in porous media or across porous baffle plates. The final terms of equation (2) account for the injection of mass at a source represented by a geometry component. uw, vw, ww refer to the fluid velocities of the source components, which will generally be non-zero for a mass source at a general moving object. u_s, v_s, w_s are the fluid velocity vectors at the surface of the source relative to the source itself. With present numerical treatments,

the fluid properties are fixed at the pre-defined values.

Since the velocity-pressure form of the governing equations (1) and (2) is used based on the finite difference method to solve the transient air-water mixed flows at the single entry flow conditions. To solve the complex interfacial flow structures for such multi-entry gully flows, the present numerical scheme uses a Renormalization Group (RNG) k-ε model to solve the complex flow phenomena. The method was proposed by Yakhot and Orzag [17] for the incompressible flows (water) can be derived from the Eqs. (3) and (4) as follows:

$$\frac{\partial(\rho k)}{\partial t}+\frac{\partial \rho uk}{\partial x}+\frac{\partial \rho vk}{\partial y}+\frac{\partial \rho wk}{\partial z} = (\mu+\frac{\mu_t}{\sigma_k})\left(\frac{\partial^2 k}{\partial x^2}+\frac{\partial^2 k}{\partial y^2}+\frac{\partial^2 k}{\partial z^2}\right)+P_k-\rho\varepsilon \tag{3}$$

$$\frac{\partial(\rho \varepsilon)}{\partial t}+\frac{\partial \rho u\varepsilon}{\partial x}+\frac{\partial \rho v\varepsilon}{\partial y}+\frac{\partial \rho w\varepsilon}{\partial z} = (\mu+\frac{\mu_t}{\sigma_\varepsilon})\left(\frac{\partial^2 \varepsilon}{\partial x^2}+\frac{\partial^2 \varepsilon}{\partial y^2}+\frac{\partial^2 \varepsilon}{\partial z^2}\right)+c_{1\varepsilon}\frac{\varepsilon}{k}P_k-c_{2\varepsilon}^{*}\rho\frac{\varepsilon^2}{k} \tag{4}$$

Where

$$c_{2\varepsilon}^{*}=c_{2\varepsilon}+\frac{C_\mu\eta^3(1-\eta/\eta_0)}{1+\beta\eta^3},\ \eta=Sk/\varepsilon,\ S=\sqrt{2S_{ij}S_{ij}}$$

The related coefficients as

$$c_\mu=0.0845,\ \sigma_k=0.7194,\ \sigma_\varepsilon=0.7194,$$

$$C_{\varepsilon 1}=1.42, C_{\varepsilon 2}=1.68,\ \eta_0=4.38, \beta=0.012$$

The geometry and boundary conditions for present simulation have been previously reported [15]. For completeness, a brief description for the boundary conditions and the simulation geometry of the test gully are provided. The geometrical scaling factor for the simulated and tested gully, as shown by Fig. 1(b), is 1:1. Thus the simulated and tested gullies have identical size and weight. Present numerical results are obtained using the fine grid cells (625,600) to attack the unsteady flow phenomena. The non-uniform mesh system is deployed with the refined grids over the regions subject to large gradient components. In this respect, the finest grid is less than 1mm for present grid system. With boundary conditions, all the solid surfaces are exceptionally subject to no-slip conditions; while the boundary conditions at the air-water interfaces have to be calculated. The upstream flow velocity (entry flow velocity) is mapping with the typical turbulent pipe flow profile with the mean-flow rate controlled at the predefined entry volume flow rate. As the outflow boundary condition is relevant to the investigation for the wave interactions with structures, the imaginative mathematical continuation for the air-water flow extends further downstream the exit port of the computational domain. This treatment is the so-called Sommerfeld radiation boundary condition;

which features a simple mathematical continuation having the form of outgoing waves:

$$\frac{\partial \phi}{\partial t} + c\frac{\partial \phi}{\partial x} = 0 \quad (5)$$

where ϕ is any quantity. With present model, ϕ refers to velocity u and positive x is directed out of the boundary and c is the local phase speed of the assumed wavy flow. Within the framework of equation (5), the mixed water flow consists of wavelike disturbances that are propagating toward the boundary. Any flow quantity ϕ at the interfacial boundary will translate across the boundary with speed c. The numerical stability conditions are satisfied by using the conservative form of the momentum equations in the discretized form as expressed by Flow-3D user manual. The time-step size used of the model is not a constant in which an optimal time step was calculated automatically based on the numerical discretizations.

Experimental uncertainties for flow rate measurements, static airflow pressures and self-depuration time are estimated according to [16]. The sources of uncertainties for these measurements are mainly attributed from the precision errors of the instrumentations. With the volume water flow rate, static pressure and lumen in the respective ranges of 20~65 L/min, 0~ -170 Pa and 35~950 Lumen, the maximum experimental uncertainties for Re_L, static airflow pressure and self-depuration time are estimated 3.8%, 1.2% and 2.3% respectively. Regarding the validation for the aforementioned numerical results, Fig. 2 compares the calculated and measured static pressures at the flow exit with single entry flow at Q_A=65L/min. Three spots over the flow exit plane at the angular locations of 165°, 180°(top) and 195° are selected to collect the numerical airflow pressures. After charging the mixed water flow into the test gully at the single entry condition with Q_A=65L/min, the airflow pressure start decreasing with temporal oscillations along the time-mean pressure descending trend due to the agitating air bubbles within in the discharged mixed water, Fig. 2. However, the favorable agreements between the measured and calculated temporal pressure variations with the maximum discrepancy of ±30% are found with the transient period so that the transient results with single flow entry approximated from the numerical scheme are further analyzed.

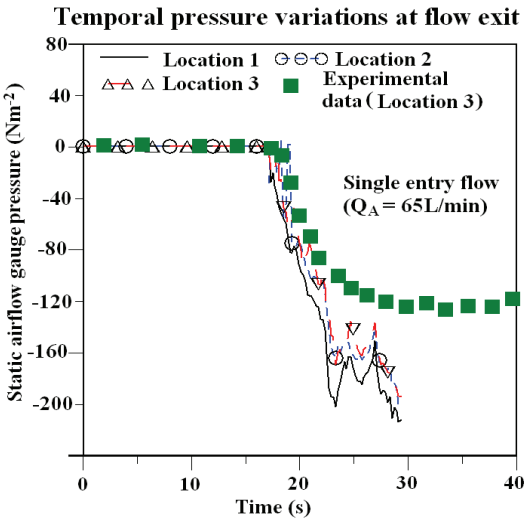

Fig. 2 Comparisons of calculated and experimental static pressures at the flow exit with single entry flow at Q_A=65L/min.

3. Results and discussion

3.1 Transient numerical flow results

Due to the complex interfacial flow structures for such multi-entry gully flows, the present numerical scheme is only capable of solving the transient air-water mixed flows at the single entry flow conditions. A set of selected numerical flow results with single entry mixed water flow is presented to provide the detailed insights of the transient flow phenomena emerged in present test gully. With this set of numerical flow results, the initial condition of the flow inlet for the mixed water flow entering the gully is assumed to have a constant volumetric water flow rate in a horizontal tube. The total computational domain is restricted within the multi-joint gully. The void air pressure in the gully is assumed at 1 atm (P_a= 1.013×10^5 N/m^2). All the computations have been carried out on a quadro-core CPU personal computer with 4 GB RAM. The computation of CPU time is approximately evaluated 25 hrs for the complete simulation of one case.

It has shown by Fig. 2 that the present scheme used one grid size to produce the acceptable results compared to the experiments data. The Flow-3D software uses high fidelity fluid dynamics, and is applied to the fields of manufacturing and science. The theoretical foundations of Flow-3D include mass conservation equation and momentum equation. Thus, it can be applied to the majority of fluid movements of all types. The grid size used in the present model is good enough as recommendation in the Flow-3D user manual.

Figure 3 depicts the 3D transient flow pattern obtained with single entry flow of Q_A=500 cm^3/s at the selected instants of t=1, 10, 50 and 100 s. Initially, the agitated water flows with wavy interfacial surfaces prevail over the free surface of the mixed-water flow at t = 1s. The water flow through present gully soon proceeds smoothly during this transient process. There is no sensible hydraulic jump developed in the upstream of the gully outlet for this test case. Free wavy surfaces constantly develop over the water plenum of present gully, indicating the complex

interfacial interactions between these multiple entrances which provide the airflow pathways into the gully.

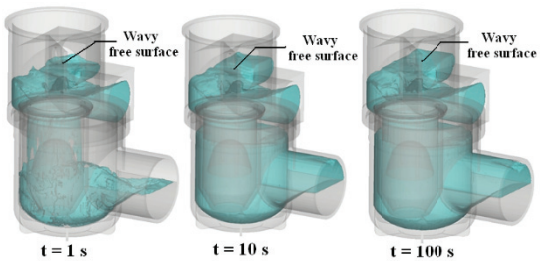

Fig. 3 3D flow patterns at various times.

Figure 4 depicts the instantaneous velocity magnitude and vectors of water flow at different time lapses during the transient process. Following the sequential flow snapshots collected in Fig. 4, the large air plenum entrained in the core of the central chamber in present gully tends to break-up, forming the disperse small-scale air bubbles in the water stream. Two swirls developed at the left and right bottoms of this gully. With the wavy free surface over the central plenum core of present gully, the air-flow is entrained from the top and side entries of present gully. A choked air bubble is formed as the water stream fills the entire flow exit as indicated by Fig. 4 at t= 50 and 100s.

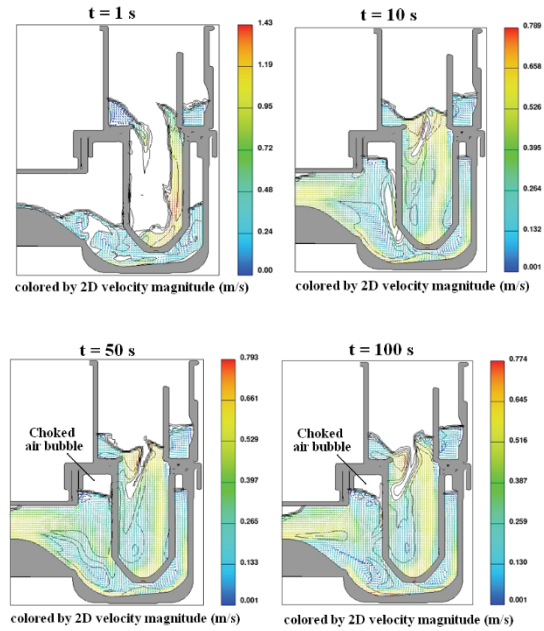

Fig. 4 Velocity magnitude and vectors at the middle plane of y=0.

Prior to the quasi-steady condition, the complex water streams through present gully as shown by Figs. 3-4 are motivated by local pressure gradients through the transient process. The transient pressure variations of water flow through present gully are collected in Fig. 5 which exhibits the process for building the static pressures in the gully to motivate the entry mixed water toward the flow exit. Initially, the low pressure mixed-water flow enters the gully with highly unstable oscillating interfacial boundaries over the entire volume of present gully. With 10 seconds lapse, the static pressure soon builds up with low pressure region emerged at the flow exit. Cross examining the fluid velocity contours depicted by Fig. 4, this low pressure flow region above the

exit bump shown in Fig. 5 corresponds to the high fluid velocity region in Fig. 4. The accelerated fluid flow through the streamlined convergent exit converts the pressure potential to the flow momentum, generating the low pressure region at the flow exit of pressure gully. Due to the reduced static pressures at the flow exit, the fluency of the mixed-water flow through present gully are considerably improved.

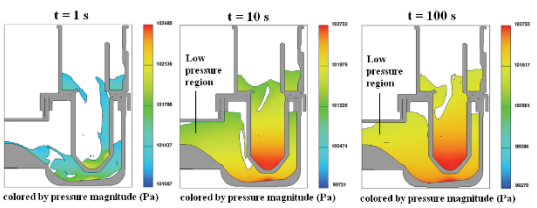

Fig. 5 Pressure contour (Pa) at the middle plane of y=0.

3.2 Experimental test results

Having revealed the basic air-water two-phase flow phenomena developed in present test gully with single entry flow by Figs. 3-5, the experimental results probe into the flow conditions with twin flow entrances. Particular attentions are addressed for the self-depuration performances detected by present newly devised optical method and the air-water flows imaged at the twin-entry flow conditions.

The sequential flow snapshots collected at t= 1, 10, 50 and 100s at Q_A=30L/min, Q_B=30L/min with single-entry flows and Q_A=Q_B=15L/min and Q_A=Q_B=30L/min with twin-entry flows are collected in Fig. 6.

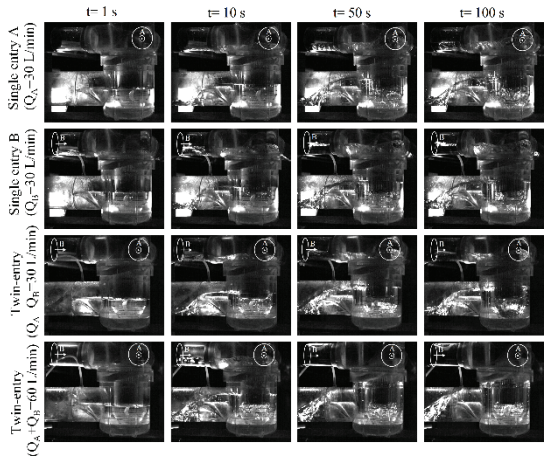

Fig. 6 Sequential flow snapshots collected at t= 1, 10, 50 and 100 s at Q_A=30L/min, Q_B=30L/min with single-entry flows and Q_A=Q_B=15L/min and Q_A=Q_B=30L/min with twin-entry flows.

Irrespective to the single or twin entry flow conditions, the air bubbles taking the typical bubbly flow structures emerge at the bottom of the central liquid pool of present gully and at the location downstream the streamlined bump, Fig. 6. With the stratified mixed water entering the gully core from the horizontal inlet pipe, the highly unstable wavy-like free surface prevails over the annular flow surrounding the central gully core. Over the top surface of such unstable wavy free-surface, the agitating water stream entrains airflow into downward the core chamber of present bully. At the bottom of central core, the impinging mixed-water stream undergoes considerable pressure variations upon impingement, leading to considerable pressure relaxations to release the entrain air from the water

stream. A cluster of small-scale air bubbles are accumulated/trapped underneath the central plenum with limited and dispersed air bubbles drifting in the downstream water stream toward the streamlined bump at the exit of present gully. With the twin entry flow condition of Q_A=Q_B=30L/min, the maximum discharged flow rate about 60~65 L/min is approaching. With the discharged flow rate approaching the maximum capacity, the water flow tends to fill the entire throat of the converging flow exit. Such criterion for setting the maximum discharge capacity of present gully is clearly demonstrated by depicting the flow images detected at the quasi-steady states with single and twin-entry flows, Fig. 7.

Figure 7 depicts the flow images detected at Q = 30, 40 and 65 L/min with single and twin entry flows. Even with the two orthogonal flow entries, namely entry A and entry B as indicated in Fig. 7, the air-water flow structures developed in present test gully follow the similar pattern. In this respect, the air-bubble cluster accumulated underneath the central core plenum with wavy-like free surfaces emerging at the top end of the central plenum and downstream the streamlined exit bump, Fig. 7. With either single or twin entry flows, the water flow fills fully the throat of the convergent flow exit at the maximum discharge capacity of 65 L/min. Further performance improvements are thus directed toward the stabilizing air-bubble agitation /segregation underneath the central plenum of present gully and/or the extending flow rate through the throat of the convergent flow exit.

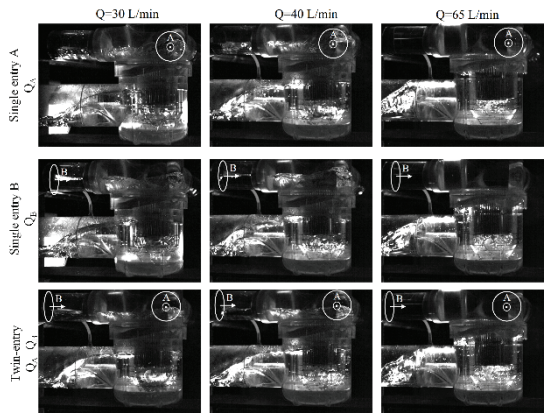

Fig. 7 Flow images detected at Q= 30, 40 and 65 L/min with single and twin entry flows.

With applications to the drainage system of a building, it is also important to minimize the unfavorable impacts on the discharged air-water flow downstream the gully. Thus the temporal variations of airflow pressure are detected at various mixed water flow rates. For present test gully, the installation of streamlined bump downstream the flow exit considerably stabilizes the air-water flows through the gully. With the total flow rate of mixed water less than the maximum discharging capacity, the temporal variations of airflow pressure downstream the flow exit of present test gully are extremely stable, which are exemplified by Fig. 8(a) in which the instant airflow pressures

recorded through the transient process after the single discharges of Q_A=40L/min or Q_B=40L/min and the twin-discharge of Q_A=20 L/min and Q_B=20L/min are compared. The stable airflow pressures at the atmospheric level are confirmed. When the single or twin flow rates reach the maximum discharge capacity of present test gully of 65 L/min, the airflow pressures become sub-atmospheric. In this regard, the airflow pressures downstream the test gully at the twin-entry flow condition of Q_A=Q_B=32.5L/min are subject to the less impact, which is followed by the single entry flow from entry B at Q_B=65L/min and the most severe impact at the single entry flow from entry A at Q_A=65L/min, Fig. 8(b). With the exit throat being fully filled by the mixed water at the maximum discharging flow rate as depicted by Fig. 7, the sub-atmospheric levels of airflow pressure are closed relevant to the entrain airflow from the flow entry. With twin-entry flows, the patterns of the interfacial flow structures in the horizontal entry pipe remain as the stratified wavy flows, enabling the airflow entrainment into the entry mixed-water flow. However, with the single entry flow at the maximum flow rate of Q_A=65L/min or Q_B=65L/min, the entire inlet pipe is filled with water flow so that the air entrainment from the incoming entry mixed water stream is considerably moderated. The differential sub-atmospheric levels between the single entry flow conditions of Q_A=65L/min or Q_B=65L/min are attributed to the discharging capacity of the air bubbles from the bubble cluster accumulated underneath the central core of present gully. When the entry flow pipe (entry B) is in parallel with the exit pipe of present gully, the better air-bubble discharge from the bubble cluster underneath the central plenum can be achieved. With the single flow entry from pipe A which is orthogonal to the discharge pipe of present gully, the strength of swirl developed underneath the central plenum seems to be weakened from the entry B scenarios. Further swirling enhancement underneath the central plenum for the hydrodynamic performances of present test gully is worthy of future investigations.

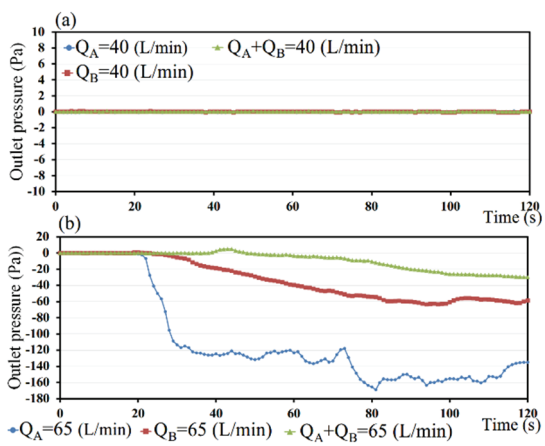

Fig. 8 Temporal variations of airflow pressure with single and twin entry flows at

(a) Q_A=40 L/min, Q_B=40 L/min and twin-discharge of Q_A= Q_B=20 L/min (b) Q_A=65 L/min, Q_B=65 L/min and twin-discharge of Q_A= Q_B=32.5 L/min.

Another aspect which is worthy of investigation is the capability of self-depuration for a multi-entry gully. The test results collected from the optical measurement method illustrated in Fig. 1 for present test gully are shown by Fig. 9 with (a) single A entry of Q_A= 20, 30, 40, 65 L/min (b) single B entry of Q_B= 20, 30, 40, 65 L/min (c) twin A and B entry with Q_A= Q_B of Q_A+Q_B=20, 30, 40, 65 L/min. As indicated by each temporal L/L_1 variations shown in Fig. 9, the self-depuration performance of present test gully is characterized as a "waiting period" followed by the exponential-like curve at each test condition. At low flow rate of Q_A=Q_B=(Q_A+Q_B)=20 L/min, the L/L_1 curves shown in the respective Figs. 9(a), 9(b) and 9(c) undergo a substantial period of waiting period during which the L/L1 ratios remain at about zero. Thus the replenishment of fresh mixed water during the waiting period is considerably limited. However, by way of momentum enrichment for the entry mixed water flow, the waiting period is consistently reduced as the discharging flow rate through the test gully increases, Figs. 9(a)-9(c). After the waiting period, the following L/L_1 ratios raise rapidly with diminished L/L_1 agitations, Figs. 9(a)-9(c). Within this particular period, the cluster of air bubbles underneath the central plenum is not yet developed so that the transparency of the scanned test gully can be rapidly improved, reflecting the effective/efficient replenishment of fresh mixed water with lesser degrees of form/frictional drags induced by the air-bubbles. Having transited through the period of rapid replenishment, the L/L_1 ratios are steadily increased at the moderate rate with the most noticeable L/L_1 agitations in this final stage. Clearly, the agitating L/L_1 ratios at the final stage are caused by the drifting air bubbles in the water stream which prohibit the effective/efficient replenishment of fresh mixed water by weakening the through flow momentum due to the enhanced form/frictional drags at the interfacial boundaries of these agitating air bubbles. The typical distributing pattern of L/L_1, which exhibits consistently for the data trends collected in Fig. 9, shows a waiting period during which the air-water flow in the gully is under development with insufficient discharging momentum for self-depuration. To overcome the partial blockage of air bubble(s) in the gully and reinforce the discharging momentum during the waiting period, the adding swirls by fitting skewed surface ribs inside the drum of a gully is worth of further investigations for design improvements of a gully. Nevertheless, as described previously, the self-depuration duration (T) is defined at L/L_1= 0.99. The various T

values obtained from the self-depuration tests are collected in Table 1.

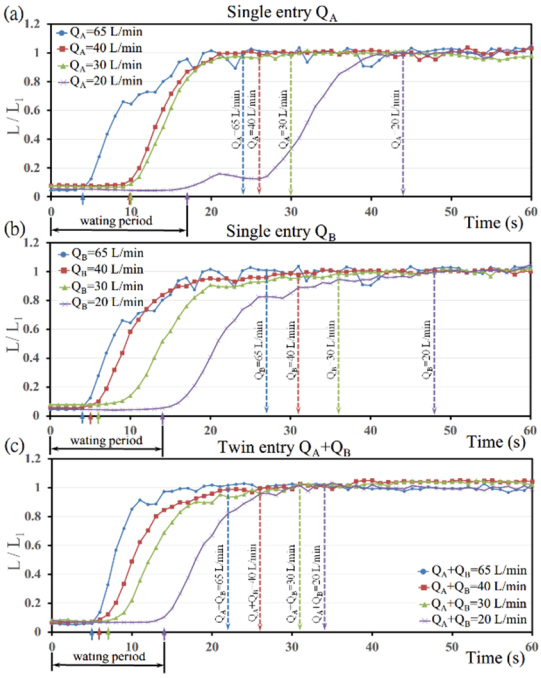

Fig. 9 Temporal variations of L/L_1 with (a) single A entry of Q_A= 20, 30, 40, 65 L/min

(b) single B entry of Q_B= 20, 30, 40, 65 L/min (c) twin A and B entry with

Q_A= Q_B of Q_A+Q_B=20, 30, 40, 65 L/min.

Table 1 Self-depuration durations (T) at single and twin entry conditions.

Q (L/min)	T (s)		
	Single entry (A)	Single entry (B)	Twin entry (A+B)
65	24	27	22
40	26	31	26
30	30	36	31
20	44	48	34

The variations of self-depuration duration (T) against the total discharge flow rate (Q) with single and twin flow entry conditions are compared in Fig. 10. At each flow entry condition, the self-depuration durations keep reducing as Q increases, Fig. 10. At a fixed Q, the order of the self-depuration durations (T) generally follow the order of $T_A > T_B > T_{A+B}$ as compared by Fig. 10. Following the consistent Q-driven T varying trends depicted in Fig. 10, three sets of empirical T correlations are devised as equations (4)-(6) as the design aid for approximating the self-depuration duration using present test gully.

$$T_A = 89.6 - 16.43\ln Q \quad \text{Single A entry} \quad (4)$$

$$T_B = 98.02 - 17.54\ln Q \quad \text{Single B entry} \quad (5)$$

$$T_{A+B} = 66 - 10.59\ln Q \quad \text{Twin A+B entry} \quad (6)$$

Justified by the consistent test results depicted in Figs. 9-10, the present newly devised optical measuring method for determining the self-depuration duration of a test gully involving complex interfacial flow structures is favorably demonstrated; which can be adopted to quantitatively assess the self-depuration duration of a gully.

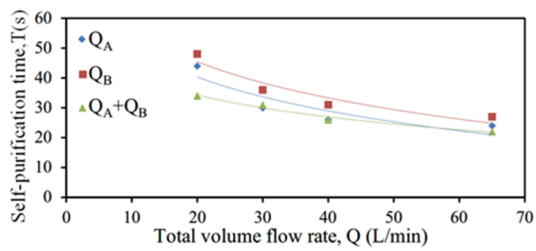

Fig. 10 Variations of self-depuration duration (T) against total discharge flow rate (Q) with single and twin flow entry conditions.

3. Conclusions

This work adopts the numerical and experimental methods to examine the hydrodynamic performances of the multi-entry gully with drainage applications for a building. The following salient remarks emerge from this study.

1. The presence of a streamlined bump downstream the flow exit of the multi-entry gully assists to stabilize the upstream air-water flow by generating the low pressure region at the convergent throat of the flow exit.
2. The entrained airflow transits into air-bubble cluster underneath the central plenum of present test gully after the impingement of the downward mixed-water stream. These agitated small-scale air bubbles increase the form/frictional drags over the interfacial boundaries to weaken the exit flow momentum for prohibiting the effective/efficient replenishment of fresh mixed water.
3. The maximum discharge capacity of present test gully at either single or twin entry conditions are limited by the choked flow at the convergent throat downstream the flow exit.
4. A newly devised optical measuring method for quantitatively determining the self-depuration duration of a gully involving complex interfacial flow structures is developed. The typical three-stage temporal L/L_1 variations constituted by the "waiting period", "rapid increase period" and "steadily moderate increase" period is disclosed for present test gully.
5. The self-depuration period at either single or twin entry condition consistently decreases as Q increases. Three set of empirical T correlations are devised to assist the relevant building applications.

References

[1] J.A., Swaffield, D.P. Campbell, (1992) Air pressure transient propagation in building drainage vent systems, an application of unsteady flow analysis, Building and Environment 27: 357-365.

[2] J.A. Swaffield, D.P. Campbell, (1995) The simulation of air pressure propagation in building drainage and vent system, Building and Environment 30: 115-127.

[3] S.W. Chang, C.-M. Hsieh, C. Y. Lin, H.-F. Liou, (2012) Air-water drainage flow through finned bend, Journal of Asian Architecture and Building Engineering 11: 177-184.

[4] J.A. Swaffield, L.B. Jack, D.P. Campbell, (2004) Control and suppression of air pressure transients in building drainage and vent systems,

Building and Environment 39: 783-794.

[5] S.W. Chang, D.C. Lo, (2009) Advances in multiphase flow and heat transfer 2: 176-215. Chapter 6 Air-Water Two-Phase Flows with Applications to Drainage System, Bentham Science Publishers Ltd.

[7] 張始偉；楊春陵；劉新豐, 浴室排水匯流裝置結構,中華民國專利新型第 M338857 號 (2008-August, 2018-January).

[8] 張始偉；楊春陵；劉新豐, 浴室排水匯流裝置結構(二), 中華民國專利新型第 M345088 號 (2008-November, 2018-June).

[9] 劉新豐；張始偉, 浴室排水匯流裝置結構(三), 中華民國專利新型第 M362254 號

[10] 張始偉；劉新豐, 浴室排水匯流裝置結構,中華人民共和國實用新型專利證書 證書號第 1392955 號 (2009-June, 2019-June).

[11] 張始偉；劉新豐, 浴室排水匯流裝置結構,中華人民共和國實用新型專利證書 證書號第 2222003 號 (2011-September, 2021- September).

[12] 張始偉；劉新豐, 浴室排水匯流裝置結構改良,中華民國專利新型第 M434797 號 (2012-August, 2021-September).

[13] EN 1253-2 Gullies for buildings – Part 2: Test methods, European standard, December 2003.

[14] CNS 14431 Q3001 油脂截留器性能試驗法,中華民國國家標準, May 2000.

[15] D.-C. Lo, S-F. Liou, S.W. Chang, Hydrodynamic characteristics of confluent unit device for drainage system, 2012 SPSEA Proceedings, pp. 271-280, 2nd International Symposium on Plumbing System in East Asia, 3rd November, 2012, National Taiwan University of Science and Technology, Taipei, Taiwan.

[16] Editorial Board of ASME Journal of Heat Transfer, (1993) Journal of Heat Transfer Policy on Reporting Uncertainties in Experimental Measurements and Results, ASME J. Heat Transfer 115: 5-6.

[17] V. Yakhot, S. A. Orszag, (1986) Renormalization group analysis of turbulence, I: basic theory, Journal of Scientific Computing 1: 3-51.